Journal of Applied Physics PERSPECTIVE scitation.org/journal/jap

Flexible thermoelectrics: From energy harvesting to human–machine interaction

Cite as: J. Appl. Phys. 133, 110901 (2023); doi: 10.1063/5.0135663
Submitted: 22 November 2022 · Accepted: 22 February 2023 ·
Published Online: 15 March 2023

Yao Wang,[1,2,a)] Lu Yang,[1] Yantao Zheng,[1] Dangxiao Wang,[3] and Yuan Deng[2]

AFFILIATIONS

[1]School of Materials Science and Engineering, Beihang University, Beijing 100191, China
[2]Key Laboratory of Intelligent Sensing Materials and Chip Integration Technology of Zhejiang Province, Hangzhou Innovation Institute, Beihang University, Hangzhou 310052, China
[3]State Key Lab of Virtual Reality Technology and Systems, Beihang University, Beijing 100191, China

[a)]**Author to whom correspondence should be addressed:** wang-yao@buaa.edu.cn

ABSTRACT

Thermoelectrics is the simplest technology applicable for direct energy conversion between heat and electricity. After over 60 years of fruitful research efforts, recent boom in flexible electronics has promoted the rapid development of flexible thermoelectrics with rising performances, discovery of new materials and concepts, unconventional device configuration, and emerging applications not possible for traditional thermoelectric (TE) semiconductors. In this *Perspective*, we first overview representative flexible TE materials, then discuss recent breakthroughs for flexible TE devices assembled from various types of TE materials employing different technical routes. They exhibit promising power generation and sensing performances, and aim for applications in wearable electronics, such as the power supply harvesting heat from body for low-power electronics, temperature sensors for tactile e-skin, and newly emerged application as a thermo-haptic device in an extended reality system.

I. INTRODUCTION

Thermoelectric effects, describing coupling between thermal and electrical phenomena, based on which thermoelectric materials realize direct conversion between heat and electricity, are recently one of the hottest topics as the demand for sustainable energy becomes the prime issue globally.[1–3] In the presence of a temperature gradient, enormous number of electrons carry both heat and entropy at an equilibrium state and can flow from a hot side to a cold side to build a potential difference, which is known as Seebeck effect. Thermoelectric generator (TEG) developed based on such principle could convert thermal energy directly to electricity, possessing superiorities in long-term supply, maintenance-free, and no moving parts. The performances of TE materials are accessed by temperature-dependent, material's dimensionless thermoelectric figure of merit defined as[4,5]

$$ZT = \frac{\sigma S^2}{\kappa} T, \tag{1}$$

where T is the average temperature of hot and cold sides, S is the Seebeck coefficient, and σ and κ are the electrical and thermal conductivities of the material, respectively.

After more than 60 years of fruitful work, thermoelectrics has established successful applications in converting the heat from the Sun, radioisotopes, automobiles, and industrial sectors to electricity. Electricity also can drive a TE device to work as a solid-state heat pump for distributed spot-size refrigeration. However, TEGs assembled from traditional solid-state inorganic semiconductors are not an economically viable solution in large-area energy-harvesting applications; instead, they have particular advantages over heat engines for small-scale implementations or applications, where maintenance is a major issue.[6] With recent boom in wearable electronics market and Internet of Things (IoTs) technique, the urgent need for long-term, portable, and maintenance-free power supply has triggered great interest in TEGs, which hold great promise to take the advantage of the temperature difference between human body and environment as the heat source to drive low-power wearable electronics realizing self-powered electronics.[7–10] Apart from power generation applications, TE-based devices have also emerging applications as part of IoT sensors monitoring the environmental temperature in extreme conditions, body temperature for health care, providing tactile sensory in human–machine interaction applications.

In this *Perspective*, we discuss recent breakthroughs for flexible thermoelectric devices (*f*-TED) assembled from various types of TE materials employing different technical routes, exhibiting promising power generation and sensing performances, and we focus on their applications in wearable electronics, such as power supply for low-power consumption electronics using energy harvesting from body heat, temperature sensors for tactile e-skin, and newly emerged application as a thermo-haptic device in an extended reality system as summarized in Fig. 1.

The primary challenge to develop wearable electronics is the mechanical mismatch between rigid electronics and soft skin. To realize flexible electronics, two main strategies, i.e., materials and structural engineering, have been extensively explored so far. Structural engineering approaches achieve stretchability through an island-bridge configuration, in which the rigid electronic components are arranged into sparse arrays ("islands") on soft substrates and connected using stretchable conductors, such as carbon-black-doped silicone or liquid metals ("bridges"). Non-stretchable materials such as metals and conductive pastes could be patterned into architectures such as serpentine traces, wrinkles, 3D arcs and helices, kirigami-inspired cutting patterns, and textiles to become stretchable interconnects. Materials engineering approaches, by contrast, employ intrinsically soft and stretchable materials that retain their electronic properties under large deformations, such as conjugated polymers, liquid metals, and composites of elastomers, as well as functional nanomaterials that can be patterned into high-density transistor arrays.[19,23,24] Since the main effort in flexible thermoelectric devices is devoted to optimize the properties of materials, recent advances in flexible TE materials have been briefly overviewed as shown in Table I and discussed first.

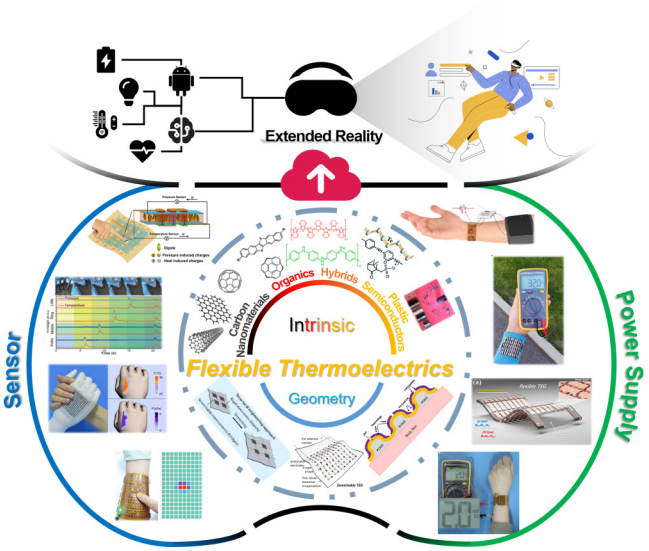

FIG. 1. Overview of representative flexible thermoelectric materials, devices, and their applications in power supply and sensors, as well as potential applications in extended reality.[11–22]

II. FLEXIBLE THERMOELECTRIC MATERIALS

A. Organic semiconductors

Conjugated polymers, as one major type of organic semiconductors, have received broad appeal as flexible thermoelectric materials due to their versatile chemical synthesis, low-cost solution processability, and exclusive mechanical robustness, which make them geometrically versatile and lightweight solutions for wearable applications.[25–43,102–104] Since the weakly bonded macromolecules with numerous degrees of conformational freedom of conjugated polymers result in complex microstructures, charge transport in such materials is contributed from electronic processes at various length scales, from molecules, interchain to domain boundaries, giving rise to generally much lower carrier mobility compared to inorganic semiconductors.[105] Yet, organic semiconductors do not typically obey the Wiedemann–Franz law, as the correlation between σ and κ is weak, suggesting that tuning free-carrier concentration via proper doping could optimize thermoelectric power factor ($PF = \sigma S^2$, σ and S have opposite dependences on carrier concentration n, leading to an optimized n for reaching the peak PF value) while keeping their intrinsically low thermal conductivity, so that figure of merit could be maximized.[28]

Take poly(3,4-ethylenedioxythiophene) (PEDOT) as an example, which has been the most widely investigated *p*-type organic thermoelectric material so far.[25–32,102,103] Precise control of the oxidation level of PEDOT:Tos and minimizing total dopant volume via removing non-ionized dopants in poly(3,4-ethylenedioxythiophene):poly (styrenesulfonate) (PEDOT:PSS) give rise to an order of magnitude enhancement in power factor from tens to hundreds of μW/m·K^2 while maintaining κ at 0.37 and 0.52 W/m·K, thus resulting in high ZT values up to 0.25 and 0.42, respectively.[28,29] In comparison, *n*-type conducting organic materials have fewer varieties and show inferior properties comparing to their *p*-type counterparts, largely owing to the small electron affinity of many organic materials, which lead to chemical instabilities of negatively charged molecules through reactions with the environment. Sun *et al.* investigated a series of metal-organic coordination polymers containing 1,1,2,2-ethenetetrathiolate (ett) linking bridge: poly[Ax(M-ett)] (A = tetradecyltrimethyl ammonium, tetrabutyl ammonium, Na^+, K^+, Ni^{2+}, Cu^{2+},M = Ni and Cu) and found that poly[K_x(Ni-ett)] with a Seebeck coefficient of −121.6 to −151.7 μV/K @ 400 K was able to achieve a ZT value of 0.2 @ 440 K, which is the first demonstrated *n*-type organic TE material.[40] The same group subsequently realized a maximum power factor and ZT values up to 236 μW/m·K^2 and 0.26, respectively, in an *n*-type small molecule aromatic-dicyanovinyl-dipyrrolo[3,4-c]pyrrole-1,4-diylidene)-bis(thieno[3,2-b] thiophene) (A-DCV-DPPTT) via a conjugated backbone modulation strategy for electronic structure and mobility tuning.[39]

B. Organic–inorganic hybrids

Apart from recent encouraging results on organic semiconductors showing ZT values approaching those of inorganic materials, organic–inorganic composites or hybrid materials provide a unique way to optimize thermoelectric properties through interface engineering in addition to the proper molecular structure design and incorporating fillers with a high electrical conductivity and a large

TABLE I. Summary on the thermoelectric and mechanical properties of representative flexible thermoelectric materials by category.

Materials	Type	S (μV/K)	σ (S/cm)	K (W/m·K)	ZT	E (MPa)	Stretchable/ Flexible	Stable temp. range	Reference
Organic semiconductors									
PEDOT:PSS/Ionic liquid	P	63.3	1594.8	0.2–0.5	0.75	…	F	290–410 K	25
PEDOT:PSS film	P	39.2	2170	0.2–0.34	0.29–0.49	…	F	…	26
PEDOT NWs/PEDOT:Tos	P	59.3	1270	0.286	0.44	…	F	…	27
PEDOT:PSS-DMSO* mixed	P	73	880	0.22	0.42	…	F	300 K	28
PEDOT:Tos	P	40	300	0.37	0.25	…	F	…	29
PEDOT:PSS fibers	P	19.2	4029.5	0.5–1	0.05–0.09	389.5	S	…	30
PEDOT:PSS-IL-WPU*	P	140	100	…	…	6.9 ± 1.7	S	298–353 K	31
PEDOT:PSS/Polymeric surfactant/ TritonX-100	P	13.4	137	0.27	…	8	S	298–379 K	32
P3HT*-TCB* treated	P	53.1	221.5	…	0.1	…	F	300–365 K	33
PANI/HCl	P	35	6.015	0.276	0.000 267	…	F	303–423 K	34
PANI film	P	20	220	…	…	…	F	20–300 K	35
PPy* nanotube film	P	17.68	9.81	0.17	0.000 571	…	F	290–370 K	36
PPy-APS*	P	10.1	2.217	…	…	…	F	…	37
SIS*/P3BT*/BCF*	P	102	0.49	0.277	0.001 26	…	S	300–393 K	38
A-DCV-DPPTT/N-DMBI	N	−665	4.9	0.34	0.23	…	F	373 K	39
Poly[K_x(Ni-ett)]	N	−151.7	63.1	0.31	0.2	…	F	220–440 K	40
2DQTT-o-OD/(2-Cyc-DMBI-Me)$_2$	N	−400	1.0	0.28	0.02	…	F	293–373 K	41
Na_x (Ni-ett)$_n$/PU*/GO*	N	−40	0.025	…	…	78 ± 8	S	298–353 K	42
PDI*	N	−167	0.5	…	…	…	F	…	43
Organic/Inorganic hybrids									
PEDOT/Bi_2Te_3	P	173	451	0.7	0.58	…	F	300 K	44
PEDOT:PSS/SnSe	P	110	325	0.25	0.32	…	F	300 K	45
PEDOT:PSS/Cu_2Se	P	50.8	1047	0.25–0.3	0.3	…	F	300–420 K	46
PEDOT:PSS/CNTs/Te	P	53	1055	0.39	0.24	…	F	300–410 K	47
PEDOT:PSS/Bi_2Te_3	P	47	1026	0.29	0.2	…	F	300 K	48
PEDOT:PSS/Te	P	163	19.3	0.22–0.3	0.1	…	F	300 K	49
PEDOT:PSS/Te-NWs	P	27.2	102.2	…	…	3300	S	…	50
$CuPc_5/Bi_{0.5}Sb_{1.5}Te_3$	P	160	1300	0.63	1.1	…	…	300–523 K	51
PAN yarns/Sb_2Te_3	P	178	750	3	0.24	…	F	300–500 K	52
PANI/Te	P	102	102	0.21	0.223	…	F	298–463 K	12
Epoxy/$Bi_{0.5}Sb_{1.5}Te_3$	P	270	114.9	…	…	…	F	300–450 K	53
SWCNT/Bi_2Te_3	N	−172	524	0.52	0.89	…	F	300–373 K	54
Cellulose Fibers/Bi_2Te_3	N	−130	148	0.4	0.38	…	F	300–473 K	55
$TiS_2(TBA^*)_{0.013}(HA)_{0.019}$	N	−170	250	0.87	0.33	…	F	300–413 K	56
C_{60}/TiS_2	N	−101	391	0.61	0.3	…	F	300–400 K	57
$TiS_2[(HA^*)_x(H_2O)_y(DMSO)_z]$	N	−78	790	0.12	0.28	…	F	298–373 K	58
N2200*/Co NW/SWCNTs	N	−45	1860	1.02	0.18	…	F	300–380 K	59
PVDF*/Ni	N	−20.6	4701	0.55	0.15	…	F	300–380 K	60
PANI/Bi_2S_3	N	−42	4.88	0.32	…	…	F	298–473 K	61
PANI/Bi_2S_3@Bi	N	−159.4	10.578	…	…	…	F	300–483 K	62
PVA*/Bi_2Te_3	N	−157.68	0.0172	…	…	…	F	…	63

*DMSO, dimethyl sulfoxide; WPU, water-borne polyurethane; P3HT, poly(3-hexylthiophene); TCB, 1,3,5-trichlorobenzene; PPy, polypyrrole; APS, ammonium peroxydisulfate; SIS, polystyrene-block-polyisoprene-block-polystyrene; P3BT, Poly(3-butylthiophene-2,5-diyl); BCF, tris (pentafluorophenyl)borane; GO, graphene oxide; PU, polyurethane; PDI, perylene diimides.

*HA, hexylammonium; TBA, tetrabutylammonium; N2200, poly{N,N0-bis(2-octyl-dodecyl)-1,4,5,8-napthalenedicarboximide-2,6-diyl-alt-5,50-(2,20-bithiophene)}; PVDF, polyvinylidene difluoride; PVA, poly(vinyl alcohol).

TABLE I. (*Continued.*)

Materials	Type	S (μV/K)	σ (S/cm)	K (W/m·K)	ZT	E (MPa)	Stretchable/ Flexible	Stable temp. range	Reference
Carbon nanomaterials									
CNT bulky paper	P	350	13.65	0.28	0.4	…	F	670–720 K	64
FCCVD* CNT sheet	P	55	813	…	…	…	F	300–570 K	65
Wet-spun CNT fiber	P	56.2	1367.8	…	…	…	F	300 K	66
s-SWCNTs films	P	68.6	1201.5	1.39	0.12	…	F	280–350 K	67
SWCNT films	P	88.4	3176.5	…	0.015	…	F	301–314 K	68
Carboxylic SWNT-based fiber	P	44	9	…	…	…	S	298–348 K	69
CNTs/Polystyrene	P	60	1250	…	0.41	…	F	300 K	70
CNTs/PEDOT:PSS	P	25	400	0.2–0.4	0.02	…	F	300 K	71
CNT/PVP*/PU	P	52	205	…	…	…	S	…	72
CNTF*/P3HT	P	92	130	…	…	…	F	293–344 K	73
SWCNTs/PANI	P	65	769	…	0.12	…	F	300 K	74
Br-doped graphene	P	38.2	4864	86.6	0.002 76	…	F	80–350 K	75
Graphene-Ecoflex	P	35	…	…	…	…	S	298–320 K	76
MWCNT/TCNQ*	P	45	8900	27.04	7.1×10^{-4}	…	F	300–623 K	77
L-MWCNT/TPU*	P	19.8	1.331	0.55	1.69×10^{-5}	26.67	S	…	78
TPP*-doped SWCNTs	N	−70.8	50.7	0.103	0.078	…	F	…	79
SWNTs with salts and crown	N	−63	69	0.12	0.07	…	F	298–313 K	80
CNT yarn	N	−56.4	7759.3	51	0.014	…	F	300–570 K	81
MWCNT/GO–NDMBI*	N	−47	994	…	…	…	F	298–373 K	82
CNTs/PEDOT:PSS/TDAE*	N	−1205	6.34	0.67	0.5	…	F	280–310 K	83
MWCNT/PEI*	N	−45	5000	20.42	6.5×10^{-4}	…	F	300–623 K	77
*FCCVD, floating catalyst chemical vapor deposition; PVP, polyvinyl pyrrolidone; CNTF, carbon nanotube forest; TCNQ, tetracyanoquinodimethane; TPU, thermoplastic polyurethane; TPP, triphenylphosphine; NDMBI, 1,3-dimethyl-2-phenyl-2,3-dihydro-1h-benzoimidazole; TDAE, tetrakis(dimethylamino)ethylene; PEI, polyethyleneimine.									
Ionic conductors-based TE materials									
PPP(PANI:PAAMPSA*:PA*)-SiO_2	P	17 900	0.187	0.477	3.74	0.01	S	…	84
WPU/EMIM:DCA*-Ionogel	P	34 500	0.0084	0.23	1.3 ± 0.2	0.63	S	…	85
PANI:PAAMPSA:PA	P	8100	0.237	0.451	1.04	0.011	S	…	86
EMIM:DCA/P(VDF-HFP)*	P	26 100	0.0067	0.176	0.75	…	F	…	87
P(AM-co-DMAEA-Q*)/EG*	P	2020	0.01	0.4	0.002 84	0.051	S	223–303 K	88
Gelatin-xKCl-m/n$FeCN^{4-/3-}$	P	17 000	…	…	…	…	S	…	89
PEO*-NaOH	P	10 000	…	…	…	…	F	…	90
[EMIM][TFSI*]/P(VDF-HFP)	N	−4000	0.002	0.136	…	1.3	F	…	91
*PAAMPSA, poly(2-acrylamido-2-methyl-1-propanesulfonic acid); PA, phytic acid; EMIM:DCA, 1-ethyl-3-methylimidazolium dicyanamide; P(VDF-HFP), poly(vinylidene fluoride-co-hexafluoropropylene); DMAEA-Q, *N*, *N*-dimethylamino ethylacrylate; EG, ethylene glycol; PEO, polyethylene oxide; TFSI, bis(trifluoro-methylsulfonyl)imide.									
Inorganic thin films									
Sb_2Te_3/polyimide	P	160	703	1.8	0.3	…	F	300 K	92
CuI thin films/PET*	P	162	143	0.55	0.21	…	F	300 K	93
$Bi_{0.5}Sb_{1.5}Te_3$/polyimide	P	229	38.9	…	…	…	F	300–475 K	94
$Bi_2Te_{2.7}Se_{0.3}$/Glass fabric	N	−165	763	0.37	0.81	…	F	300–350 K	95
Bi_2Te_3/Glass fabric	N	−136.9	549.2	0.93	0.33	…	F	300–350 K	96
Bi_2Te_3/polyimide	N	−233	500	…	…	…	F	278–373 K	97
Ag_2Se/Nylon	N	−140	497	0.478	~0.6	…	F	300–453 K	98
*PET, polyethylene terephthalate									
Plastic semiconductors									
$(AgCu)_{0.998}Se_{0.22}S_{0.08}Te_{0.7}$	P	270	70	0.25	0.68	…	F	300–340 K	17
$(Ag_{0.2}Cu_{0.8})_2S_{0.7}Se_{0.3}$	P	400	2000	0.55	0.42	…	F	298–800 K	99

TABLE I. (*Continued.*)

Materials	Type	S (μV/K)	σ (S/cm)	K (W/m·K)	ZT	E (MPa)	Stretchable/ Flexible	Stable temp. range	Reference
$Ag_2S_{0.5}Se_{0.45}Te_{0.05}$	N	−136	270	0.33	0.44	…	F	298–330 K	100
$Ag_{20}S_7Te_3$	N	−100	450	0.5	0.3	…	F	300 K	101
InSe	N	−500	0.87	1.6	0.034	…	F	300–725 K	99
Ag_2S	N	−1051	1.02×10^{-3}	0.54	6.3×10^{-5}	…	F	298–449 K	100

Seebeck coefficient. Since the presence of interfaces offers new opportunity to decouple the thermoelectric parameters via interfacial effects, the performances of hybrids are capable of exceeding those of individual components.[12,44–53,55–63,106–109] For example, See *et al.*[49] first reported a room temperature ZT ∼0.1 achieved in a polymer-nanocrystal nanocomposite composing of a tellurium core functionalized with PEDOT:PSS, whose maximum power factor is 70.9 μW/m·K^2, electronically outperform both PEDOT:PSS (PF ∼ 0.05 μW/m·K^2) and unfunctionalized Te nanorods (PF ∼ 2.7 μW/m·K^2) while retaining a polymeric thermal conductivity (0.22–0.3 W/m·K). Subsequent investigation reveals that a highly conductive volume of polymer exists at the polymer and inorganic nanofiller interface where carrier transport occurs predominantly.[108]

Our work on conducting polymer polyaniline (PANI)-based nanocomposites further reveals the significance of organic/inorganic interface design for high-performance TE materials. The formation of effective interface relies on an additional chemical or physical interaction between the polymer and fillers. For example, Te has high S of ∼400 μV/K and is hexagonal, containing van der Waals force between Te atom chains, which provides intermolecular interaction with conjugated chains of PANI. Such interaction also enables the ordered conformation of PANI chains surrounding Te nanorods, providing a high-speed carrier transport channel and resulting in an increase in electrical conductivity from 64.8 S/cm for the pristine PANI to 102 S/m for the hybrid. Meanwhile, the efficient phonons scattering at the organic/inorganic interface due to the acoustic mismatch between Te and the polymer preserves the thermal conductivity at a rather low level of 0.2 W/m·K. Thus, a high ZT value of 0.156 at 313 K and a maximum of 0.233 at 383 K have been realized in a simple PANI/Te nanorod hybrid system.[12] We subsequently introduced third-phase multiwalled carbon nanotubes (MWCNTs) to partially reduce the content of scarce Te element without deteriorating TE properties. MWCNTs can form molecular interaction with PANI chains via π–π interaction, which brings more interfacial volume in a ternary system, and the energy barriers formed at multiple interfaces among constituents result in energy-filtering effect to enhance S simultaneously. Twice the power factor value of ∼54.4 μW/m·K^2 for ternary PANI/MWCNT/Te as that for binary PANI/Te (PF ∼ 27.9 μW/m·K^2) at the same Te content has been obtained.[109] Besides, MWCNTs could alleviate the brittleness brought by the high-volume fraction of inorganic fillers and enhance the mechanical flexibility and stability of hybrids, which is important for device construction.

Regarding the fabrication of practically working thermoelectric devices, it is essential to develop matched *p*- and *n*-type TE materials. Compared to *p*-type hybrid materials, only few *n*-type organic composites have been reported. Wan *et al.* reported *n*-type organic intercalated layered TiS_2 and its inorganic/organic hybrids that showed promising TE performances achieving a high ZT of ∼0.33 at 413 K.[56,58] Since most of the conducting polymers are *p*-type, it becomes a great challenge if combining *n*-type inorganic fillers could transform a *p*-type polymer into an *n*-type composite. The key is to enhance the concentration or mobility of dominant carriers from fillers or to suppress the transport of holes in the polymer. We, thus, developed a simple vacuum thermal treatment process to reduce the carrier concentration of a *p*-type PANI matrix via partially cross-linking polymer chains and reducing the doping level, so that the *n*-type Bi_2S_3 nanorod filler with S ∼ −450 μV/K dominated carrier transportation; finally, a stable *n*-type PANI-based hybrid with S ∼ −42.8 μV at room temperature has been successfully obtained.[61]

C. Carbon nanomaterials

Carbon nanomaterials, such as carbon nanotubes and graphene, have rich electrical, optical, thermal, chemical, and mechanical properties and have been extensively studied in the fields of energy conversion, storage devices, catalysts, and biosensors. Carbon nanotubes become particularly attractive flexible thermoelectric materials, owing to their compliance to high-throughput solution-phase fabrication routes, magnitude higher than $\sigma \sim 10^4$–10^5 S/m compared with organic materials, moderate Seebeck coefficient in the order of 10–10^2 μV/K and promising PF around hundreds of μW/m·K^2 with some single-walled carbon nanotube (SWCNT) buckypapers even exceeding 1 mW/m·K^2, as well as their unique chemical and physical properties that facilitate equivalent transport of electrons and holes.[64–69,110] For example, Blackburn and co-workers demonstrated that the large power factor, i.e., higher than 700 μW/m·K^2, could be achieved in both *n*- and *p*-type highly pure semiconducting SWCNT networks.[67]

Carbon nanotubes are also ideal candidates for thermoelectric composites, which can provide a platform for exploring high-performance flexible TE materials. For instance, Tai *et al.* developed a flexible SWCNT network with ordered Bi_2Te_3 nanocrystals anchored on, exhibiting a high power factor of ∼1600 μW/m·K^2 and a maximum ZT of 0.89 at room temperature through a strong phonon scattering effect.[54] When CNTs are blended with conducting

polymers, substantially improved power factors have been reported by different research groups.[70–83,111–115] For example, an optimal power factor of 157 μW/m·K^2 was obtained in poly (3,4 ethylenedioxythiophene)/CNT hybrids,[113] higher PF of ~526 μW/m·K^2 was reported in 60 wt. % SWCNT/PEDOT:PSS nanocomposite,[114] and an ultrahigh PF of ~2710 μW/m·K^2 at room temperature was reported in PANI/graphene-PEDOT:PSS/PANI/double-walled nanotube-PEDOT:PSS multilayer structure by Cho *et al.*[115] These encouraging results demonstrate that composites of CNTs with polymeric or inorganic TE materials can potentially decouple electrical and thermal conductivities by introducing interfaces that provide more facile paths for electrons' transfer while scatter phonons, as well as an opportunity to utilize carrier energy filtering to decouple the thermopower (the absolute value of the Seebeck coefficient) and electrical conductivity.

D. Inorganic thin films and emerging materials

So far, properties of state-of-art organic TE materials cannot yet compete with those of inorganic bulks, such as benchmark TE materials working at room temperature, Bi_2Te_3 and Sb_2Te_3,[116] and then fabricating inorganic films onto flexible substrates to overcome the problem of material rigidity becomes another option to realize high-performance flexible TE materials. For example, Cho *et al.*[96] developed a screen printing technique to synthesize Bi_2Te_3 (*n*-type) and Sb_2Te_3 (*p*-type) thick films on a glass fabric, whose ZT values are 0.33 and 0.28, respectively. Shin *et al.*[95] identified a suitable binder additive methyl cellulose for screen printing, high room-temperature ZT values of 0.65 for *p*-type $Bi_{0.5}Sb_{1.5}Te_3$ and 0.81 for *n*-type $Bi_2Te_{2.7}Se_{0.3}$, respectively, have been obtained via minimizing the negative impact from the binder on the electrical transport of screen-printed TE layers. Cai *et al.*[98] developed the Ag_2Se nanowire film on nylon membrane, showing both good TE properties and excellent flexibility, with an ultrahigh power factor of 987.4 μW/m · K^2 and an estimated ZT of ~0.6 at 300 K, whose PF is one of the best values reported for flexible *n*-type materials.

Quite recently, a series of inorganic semiconductors with exceptional room-temperature plasticity have been discovered in succession by Shi and co-workers, including Ag_2S[13] and InSe single crystals,[117] opening a brand new avenue toward overcoming the dilemma between deformability and electrical properties. They reported the thermoelectric properties of plastic *n*-type Ag_2S-based alloys with a high ZT of 0.44 at 300 K and 0.63 at 450 K.[96] Furthermore, the first *p*-type plastic inorganic TE material $(Ag_{0.2}Cu_{0.8})_2S_{0.7}Se_{0.3}$ has been realized via Cu alloying, showing a maximum ZT of 0.42 at 800 K; moreover, by introducing a tiny amount of Cu vacancies, the ZT could be further enhanced to 0.95 at 800 K.[99]

Apart from the Seebeck effect in electronic conductors when subjected to the temperature gradient, thermodiffusion of ions in electrolytes yields ionic Seebeck coefficients (also known as Soret effect). Recent emerging exploration of the ionic thermopower through the Soret effect in polymer electrolytes leads to a surprisingly high $\Delta V/\Delta T$ (~10 mV/K), promoting a new research direction for thermal energy harvesting and ultrasensitive heat sensing.[84–90] This effect is particularly pronounced at high humidity due to faster ion transport in liquid/electrolyte media. Contrary to the Seebeck effect originated in electronic conductors, the thermodiffused ions remain confined in materials instead of being extracted by electrodes, making these materials more suitable for capacitor-like or thermocell applications instead for continuous power generation. For more in-depth discussion on emerging unconventional TE materials, we refer the readers to a recently published review by Fabiano *et al.*[6]

III. FLEXIBLE THERMOELECTRIC DEVICES

A. Configuration of TE devices

Configuration of a thermoelectric device using inorganic thermoelectric materials is well-established, with commercial products for both power generation and thermal management applications. For a typical TE module, it consists of alternating *p*-type and *n*-type TE legs electrically connected in series over a substrate that is patterned with electrical contacts, in which the thermal gradient across the material is perpendicular to the substrate, as shown in Fig. 2(a). While for flexible TE modules made from many organic and hybrid materials, they are solution-processed and such perpendicular geometry is not well suited; instead, most reported thin-film TE devices employ in-plane design to build sufficient temperature difference to generate thermopower as shown in Fig. 2(b).

Take a thermocouple with an internal resistance R subject to a temperature gradient of $\Delta T = (T_H - T_C)$ for consideration, assuming that the heat propagating from the hot to the cold side can only pass through thermoelectric legs and that the connection junction of the metal and TE legs has a negligible electrical and thermal resistance, it will generate an open-circuit voltage $V_{OC} = S\Delta T$, where $S = |S_P - S_N|$. When the thermocouple is coupled with a load resistance R_L, current $I = S\Delta T/(R + R_L)$will be generated, and the maximum output power is achieved as the resistance of load R_L equals internal resistance R,

$$P_{\max} = V_{OC}^2/4R. \tag{2}$$

Output power density ($p = P/A$, A is the substrate area for the device in perpendicular geometry) or normalized output power density ($P/A\Delta T^2$) is employed to evaluate the output performance excluding the geometry and temperature dependency. The efficiency η of the thermoelectric generator is the ratio between the

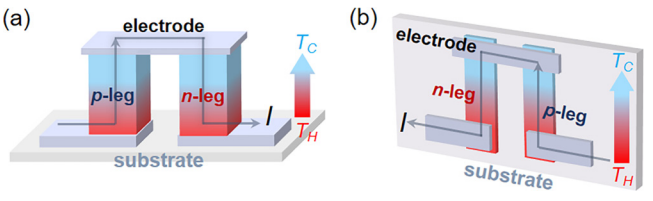

FIG. 2. Typical configurations of thermoelectric devices categorized by the direction of thermal gradient across the material with respect to the substrate: (a) Perpendicular; (b) Parallel.

electrical power output P and the thermal power input Q_H,

$$\eta = I^2 R_L \Big/ \left(ST_H I + \kappa \Delta T - \frac{1}{2} I^2 R \right). \quad (3)$$

For the thermoelectric device, its energy conversion performance is dependent not only on thermoelectric material properties, but also on the device architecture, including the leg geometries, the fill factor (the amount of space in a module taken up by thermoelectric elements), as well as the electrical and thermal matching conditions. For example, increasing the leg length allows larger ΔT across the thermoelectric generator but increases the internal resistance leading to increased Joule heating losses and compromise in P_{max} and η.

Even though flexible TE materials generally have a low power factor, flexible thermoelectric devices (f-TEDs) actually are competitive in low-temperature applications that are impractical for rigid inorganics, such as wearable energy harvesting from body heat or emerging applications such as thermal sensing and temperature feedback in human–machine interaction. They also meet other requirements from wearable electronics, such as tailored device architecture, low-energy processing, and personal comfort. The flexibility in the device design further provides the possibility for improving performance and efficiencies beyond those of traditional designs by using unconventional geometrical architectures.

B. Solution processed

As demonstrated in Fig. 3(a), solution processing enables low-cost approaches for wearable devices, such as roll-to-roll, inkjet, and screen-printing.[112,118–121] Furthermore, various creative methods have been developed to realize customizable 3D architecture from a 2D film as illustrated in Fig. 3(b), such as corrugated, rolled, or origami, so that the thermal gradient direction turns to perpendicular to the substrate to make full use of the area of heat sources.[122,123] For example, Jang *et al.* spray-printed the

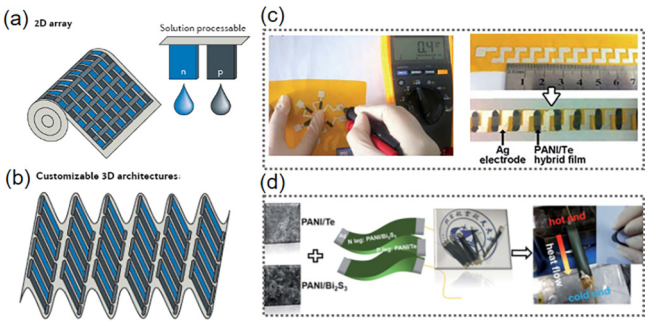

FIG. 3. Schematic illustration on the solution processed f-TED in different structures. (a) Solution-processable p-type and n-type organic thermoelectric materials printed in a roll-to-roll process. (b) 2D arrays transformed into flexible and lightweight 3D structures ideal for customized wearable applications.[124] (c) Planar structured f-TEDs fabricated from a p-type PANI/Te hybrid film.[12] (d) Zigzag-structured f-TEG integrated from both p-type and n-type PANI-based hybrid films.[61]

CNT/P3HT nanocomposite onto a polyimide (PI) substrate with a parallel TED pattern, where 41 single p-type TE legs were connected in series by printed silver electrodes, presenting a power generation performance with open-circuit voltage $V_{OC} \sim 41.8$ mV and $P_{max} \sim 32.7$ nW at $\Delta T = 10$ K.[112] Adachi *et al.* developed perpendicular structured TEG from solution-processed p-type P3HT doped by Fe^{3+}-$tos_3 \cdot 6H_2O$ micrometer thick films patterned by a photo-etching technique into a module consisting of 48 single-type TE legs, which could output a power of 2.5 μW at $\Delta T \sim 35$ K.[121] Based on our solution cast PANI-based hybrid films, f-TEDs could be assembled in various patterns and configurations via screen-printing or being tailored into desired shape via laser processing and integrated compactly into zigzag geometry as shown in Figs. 3(c) and 3(d), respectively. The function of the f-TED as a temperature sensor was demonstrated via a finger touch generated voltage of 0.4 mV. The planar structured f-TED printed on the PI substrate could also be easily rolled up and packaged into a cylindrical device generating microwatt magnitude power,[12] while the zigzag-structured f-TEG assembled from n-type PANI/Bi_2S_3 and p-type PANI/Te hybrid films showed lasting and stable output voltage with a thermopower of 224.4 μV/K per couple over a wide temperature range (from room temperature to 473 K), even comparable to inorganic Bi_2Te_3/Sb_2Te_3 thin film devices.[61]

Despite the exciting progress made for intrinsically flexible TE materials-based devices, when looking at their electrical output performances, the power density generally varies from magnitude of nW/cm^2 to several μW/cm^2 and the normalized power density around magnitude of nW/cm^2·K^2, in sharp contrast to the high power density of a few W/cm^2 achieved in inorganic semiconductors-based TEGs. These f-TEDs are still far from been satisfied functioning as practical power generators, owing to the insufficient power factor, large internal resistance, as well as great energy loss during the conversion process.

C. Polymer encapsulated

Another drawback for solution-processed f-TEDs in the planar structure is the long response time due to the long and thin TE leg as the heat and current diffusing route. So far, little achievement has been made on a vertical flexible TE device, probably owing to the difficulty in densely building up the TE device using organic TE materials exceeding certain thickness, i.e., 1 mm. Considering the difficulties for most organic materials to build a 3D architecture to match the thermal impedance and deliver practical power when harvesting heat from human body, an alternative strategy, i.e., integrating inorganic bulk TE materials into f-TEDs, has been developed, where the key technical issue is to make flexible interconnection with low resistivity and high mechanical stability.

For example, Öztürk *et al.* have developed an entirely different approach and devised a novel packaging solution as shown in Fig. 4(a), which employs high-quality bulk thermoelectric legs from commercial products embedded in a stretchable elastomer, and a eutectic alloy of gallium and indium (EGaIn) is used as a stretchable low-resistivity interconnect between the legs, so that high TE properties and flexibility have been realized simultaneously for the f-TED.[125] Chen *et al.* developed stretchable TEG employing wavy serpentine interconnects to integrate all the units consisting of

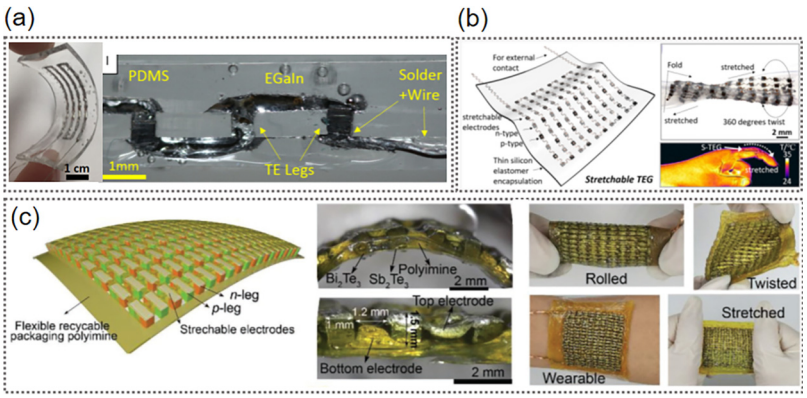

FIG. 4. Design on stretchable TEGs via elastic polymers encapsulation. (a) Photos of *f*-TEG for body temperature harvesting and illustration on the encapsulated device structure.[125] (b) Stretchable TEG integrated with wavy serpentine interconnects suitable for various complex and dynamic surfaces of heat sources.[18] (c) Illustration on the architecture of recyclable, healable, and stretchable TEG and its mechanical deformability.[126]

hot-pressed nanolayered *p*-type Sb_2Te_3 and *n*-type Bi_2Te_3 thermoelectric couple arrays and embedded in an Ecoflex elastomer as shown in Fig. 4(b).[18] We recently further developed this approach via employing dynamic covalent thermoset polyimine as the encapsulating material, endowing the TEG with additional healable and recyclable capabilities, whose merits are important considering the consumption of large amount of low abundance Te element in commercial TEGs. A recyclable, healable, and stretchable TEG, integrating 200 pairs of commercial n/p Bi_2Te_3 and Sb_2Te_3 TE legs, intrinsically stretchable and self-healable liquid metal EGaIn interconnects, encapsulated in dynamic covalent thermoset polyimine by employing low-cost and scalable laser processing, screen printing, and flexible packaging techniques has been demonstrated [see Fig. 4(c)].[126]

D. Fabrics

Integrating a power generator with textile fabrics offers a promising solution to powering personal electronic devices. Ideally, a wearable power generator should not only convert surrounding energy into electrical energy, but also be comfortable to wear, breathable, nontoxic, light-weight, and even washable, for multiple uses.[52,127–130] Kim *et al.*[52] described the fabrication of flexible, woven, and knitted textiles based on electrospun polymer nanofiber cores that were coated with *n*- and *p*-type semiconductor sheaths (Bi_2Te_3 and Sb_2Te_3, respectively) and twisted into flexible yarns. TE textiles were then fabricated by either knitting or weaving *n*- and *p*-type TE yarns into zigzag- or garter-stitch weaves that electrically connect segments in series and in parallel, or yarns containing alternating *n*- and *p*-type segments (linked by metallic interconnects) were woven in one direction and separated by insulating yarns as demonstrated in Fig. 5(a). These textile designs, contain *n*- and *p*-type regions that alternate in the textile thickness direction, are suitable for through-thickness thermal energy harvesting. Wang *et al.*[128] developed π-type thermoelectric modules woven from acrylic fibers wrapped alternately doped carbon nanotube fibers. Then these TE modules were interlocked alternately in certain patterns designed to successfully woven into a 3D TEG as illustrated in Fig. 5(b). The TE modules are self-standing to match the direction of the heat flow and have both high power generation ($70\ mW/m^2$ @ $\Delta T = 44\ K$) and excellent stretchability (~80% strain). Zhang *et al.* reported a strategy to produce inorganic semiconductors *p*-type $Bi_{0.4}Sb_{1.3}Te_3$ and *n*-type $Bi_2Te_{3.3}Se_{0.2}$ segments-based hierarchically ternary coaxial TE strings at large scale for manufacturing highly mechanically stable, stretchable, breathable and washable woven thermoelectric textiles by a textile machine as shown in Fig. 5(c), which possess good stretchability (100% elongation), flexibility (bending radius of 2 mm), washability (420 washing cycles), and output power density of $0.58\ W/m^2$ at a temperature difference of 25 K.[129]

E. Thermal interface design

Despite direct utilization of human body heat via wearable TEGs to serve as a long-term power source in self-powered wearable electronic systems is very promising, practically, the output performances of wearable TEGs worn on human body are far below those tested under fixed temperature differences.[131,132] This is largely owing to the severe thermal loss between human skin and TEG, which causes rather small practical temperature difference built across the two ends of TEG (i.e., usually no more than 1 °C), resulting in a low output voltage. Thus, it is of crucial importance for the TEG to form a good thermal contact with skin in addition to optimizing its thermoelectric performances.[133,134] Yet, the complex geometry of skin, soft mechanics, and low and uneven heat flux raise a big challenge on the thermal interface design for wearable TEG.

Generally, high thermal conductivity and low thermal resistance are critical for efficient thermal transport between TEG and contacting subject, while low-κ of TE legs is necessary to maintain the temperature difference. For *f*-TEG integrated from rigid inorganic TE legs encapsulated in elastomers such as polydimethylsiloxane (PDMS), the low thermal utilization efficiency is mainly caused by the low thermal conductivity of encapsulation materials, which results in high thermal resistance between human skin and TEGs.[125,135,136] To address the issue, strategies to enhance the thermal conduction capability of the encapsulating elastomers have recently been adopted. For example, Lee *et al.*[137] developed a soft heat conductor via magnetic field-assisted metal particles assembling along the thermal gradient direction in the elastomeric substrate to significantly enhance the heat transfer from the heat source to TEG. Ozturk *et al.*[138] added both graphene nano-platelets and EGaIn liquid metal into a silicone elastomer to reduce the parasitic thermal resistance of the encapsulation layer and serve as a heat spreader simultaneously. They further optimized filler

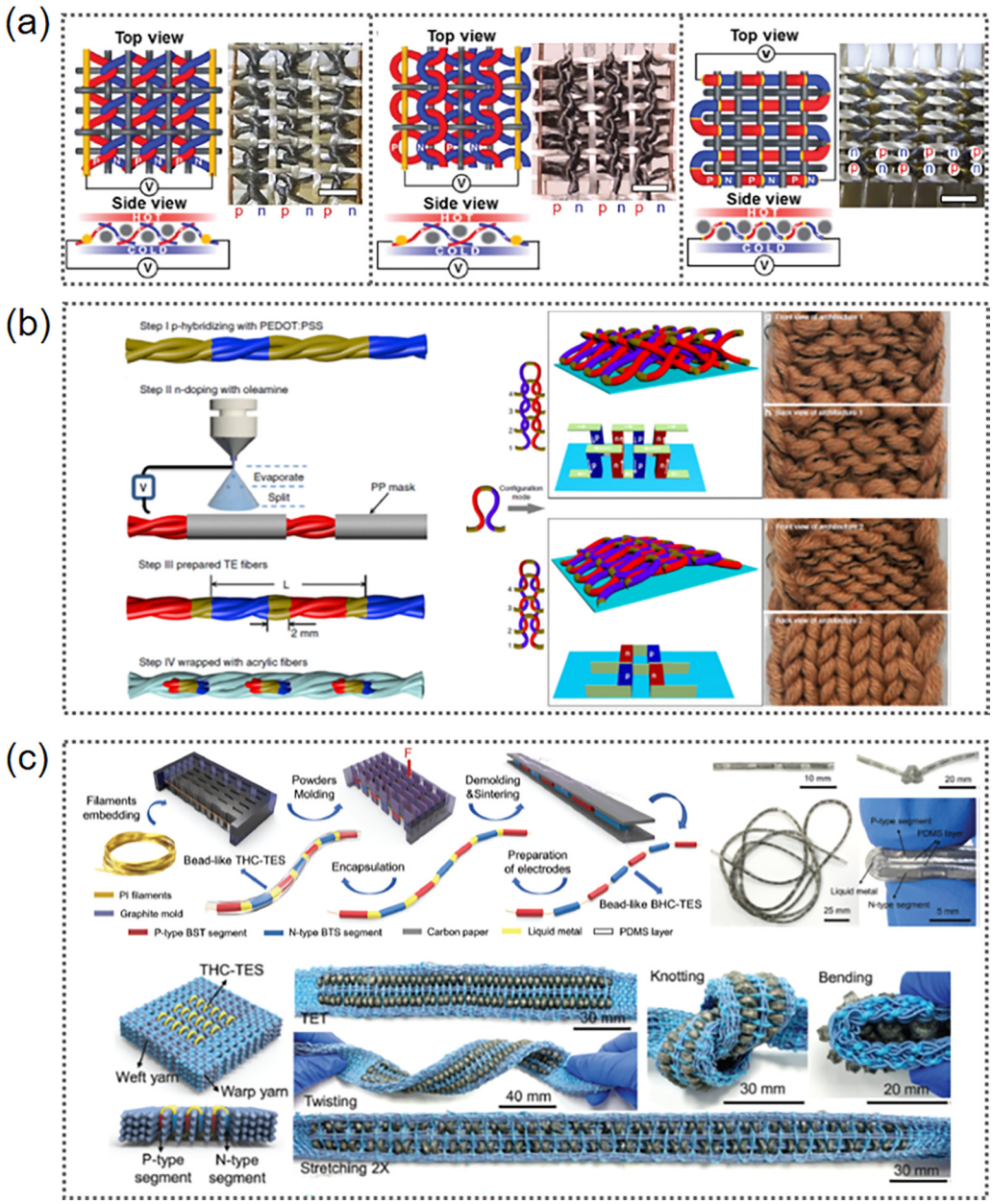

FIG. 5. Demonstrations on *f*-TEGs integrated with fabrics. (a) Schematic illustrations on the textile topologies of zigzag-stitch, garter-stitch, and plain-weave used to harvest energy from a through-thickness thermal gradient and corresponding photographs of TE textiles made from Bi_2Te_3/PAN and Sb_2Te_3/PAN yarns, respectively.[52] (b) 3D TEG textiles woven from π-type CNT fiber-based modules.[128] (c) Woven TE textiles from inorganic TE segments-based bead-like strings.[129]

materials between thermoelectric legs with ultralow thermal conductivity silica aerogel/PDMS composite to suppress the heat leakage through the TE legs that have times higher thermal conductivity than that of encapsulation elastomer.[134]

By contrast, studies on the thermal interface for organic TE materials-integrated *f*-TEGs have been few. Our recent work demonstrated that via rational thermal interface design together with overall optimization of the TEG, an efficient body temperature harvester could be realized.[14] The thermal resistance model employed for the TEG worn skin is shown in Fig. 6(a), where the heat flows from the heat source (T_H), i.e., skin, through thermal resistances of the hot side (R_H), TE leg (R_{leg}), and the cold side

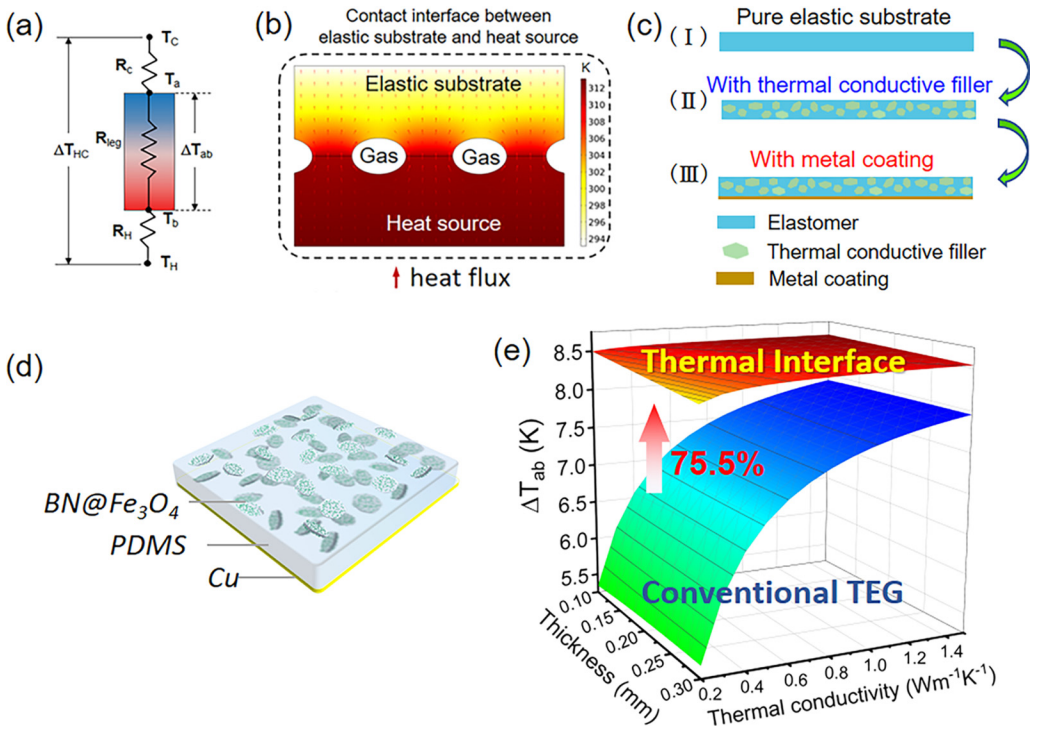

FIG. 6. Thermal interface design for high-efficiency thermal energy utilization in *f*-TEG. (a) Thermal resistance model for a single TE leg. (b) The finite element analysis (FEA) of heat transfer in the contact interface between the elastic substrate and the heat source. Schematic illustrations on (c) thermal interface material design and (d) PDMS/BN@Fe_3O_4/Cu thermal interface layer. (e) Comparison on FEA simulations on ΔT_{ab} across the TEG with/without metal coating at hot end and their variations with thicknesses and thermal conductivities of the thermal interface material.[14]

(R_C) to the cold environment temperature (T_C). The overall temperature difference utilization ratio φ_{th} is expressed as the built temperature difference across two ends of TEG (ΔT_{ab}) over the temperature difference between the hot and cold end (ΔT_{HC}),[128]

$$\phi_{th} = \frac{\Delta T_{ab}}{\Delta T_{HC}} = \frac{R_{leg}}{R_H + R_{leg} + R_C}, \tag{4}$$

where R_H includes the thermal resistances of the bottom electrode (R_e), the elastic substrate (R_s), and the thermal contact resistance (R_{TCR}) of the contact interface between the hot end of TEG and the skin. Finite element analysis (FEA) on heat flux transfer between the elastic substrate and the heat source considering the existence of microscale unevenness of the solid surface for the real contact is shown in Fig. 6(b), and the simulation result clearly indicates a large temperature drop occurring at contact interfaces caused by R_{TCR}.

The R_{TCR} can be determined as follows according to previous studies,[133,139–141]

$$R_{TCR} = \frac{(\sigma/m)}{1.25 \cdot A \cdot \kappa_s \cdot (P/H_C)^{0.95}}, \tag{5}$$

where σ is the root mean square of surface roughness, m is the average surface asperity slope, A is the macroscopic contact area, κ_s is the harmonic mean thermal conductivity, P is the applied pressure, and H_C is the micro-hardness of the substrate. The effects of these parameters on R_{TCR} for the TEG/skin could be well established and utilized to guide the design of the thermal interface. We, therefore, have designed a thermal interface material via incorporating Fe_3O_4 nanoparticles decorated high thermal conductivity boron nitride (BN) microplates aligned by the magnetic field along the heat dissipation direction into the PDMS matrix, together with a Cu metal layer coated on the surface of the PDMS/BN@Fe_3O_4 composite as illustrated in Figs. 6(c) and 6(d).[14] Such design has two important features, one is the alignment of BN microplates along the heat transfer direction and the other is the highly thermal conductive Cu layer to reduce the thermal resistance, so that the thermal transfer capability between human skin and TEG has been significantly boosted. The final *f*-TED integrated from the highly porous organic TE legs with the PDMS/BN@Fe_3O_4/Cu thermal interface layer eventually enables the establishment of a large temperature difference across the two ends, i.e., 8.6 K at a given $\Delta T_{HC} = 10$ K, higher than 4.9 K of the routine TE device without thermal interface optimization as demonstrated in Fig. 6(e).

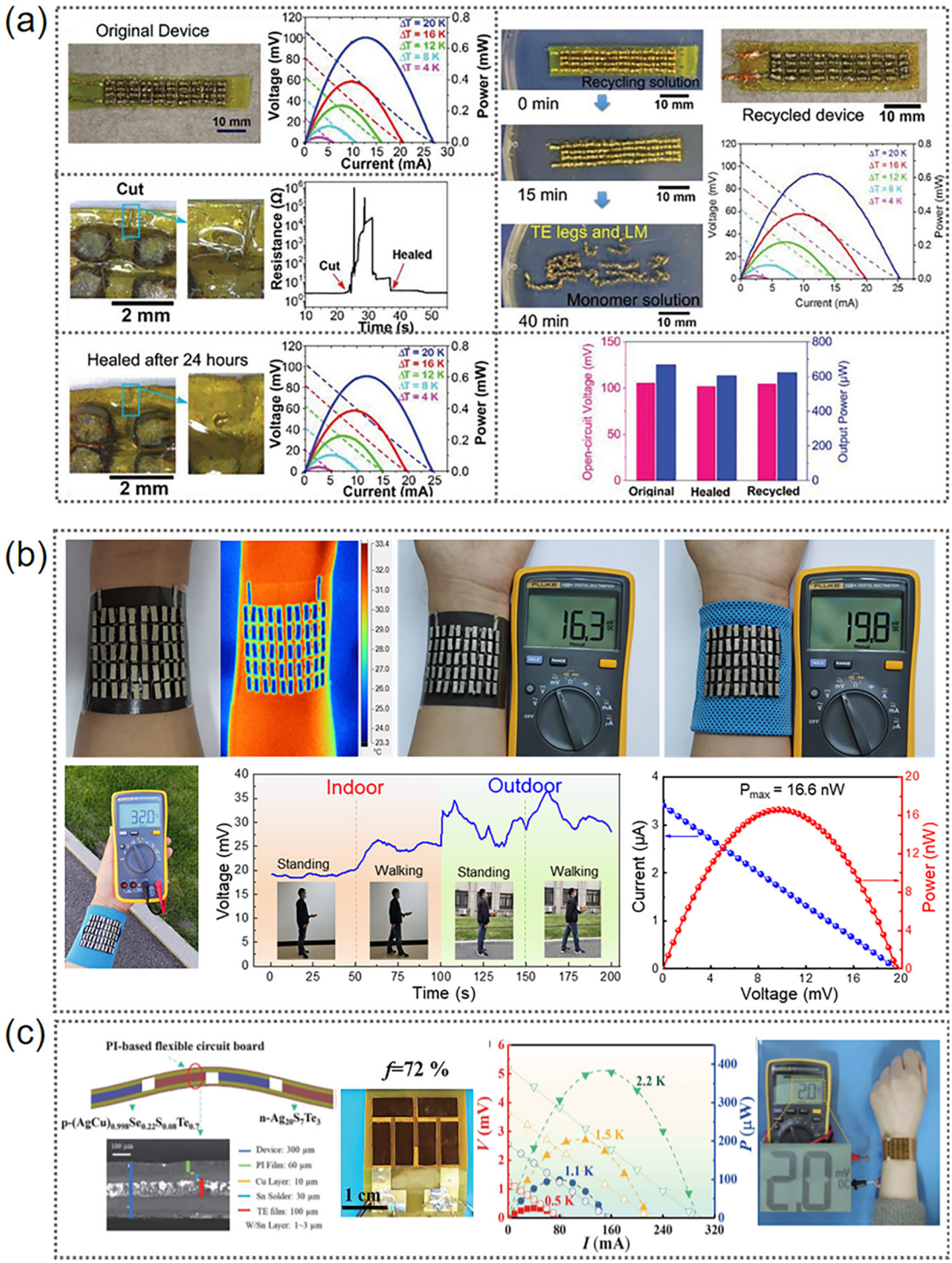

FIG. 7. Demostrations of *f*-TEGs applied in thermal energy harvesting. (a) Output performances of recyclable, healable, and stretchable high-power TEG.[126] (b) Body temperature harvesting performances of all-organic TEG.[14] (c) Output performances of super-thin flexible TE devices based on ductile semiconductors $(AgCu)_{0.998}Se_{0.22}S_{0.08}Te_{0.7}/Ag_{20}S_7Te_3$ under small temperature differences and adhered to skin, respectively.[17]

IV. THERMOELECTRIC APPLICATIONS

A. Energy harvesting

TE materials have so far been successfully applied in distributed power generation and active spot-size heat management given their unique technical advantages. When the TE devices turn from rigid to flexible, their application range could be extensively broadened. As a major example, *f*-TEGs are particularly suitable as long-term, maintenance-free, and portable power supply for wearable electronics by harvesting body heat. For example, the recyclable, healable, and stretchable TEGs we developed from commercial Bi_2Te_3 and Sb_2Te_3 TE legs show excellent TE performance with a normalized output power density up to 1.08 $\mu W/cm^2 \cdot K^2$, mechanical stretchability 50%, high reliability and stability under cyclic deformation, as well as healing and recycling capabilities as demonstrated in Fig. 7(a). After healing and recycling, the TEGs show output performance comparable to original devices. This work provides a solution for achieving both high power and mechanical compliance of TEG as well as endowing it with sustainable energy conversion ability.[126] Since the large thermal resistance between *f*-TEG and skin has severely impeded thermal energy utilization, when an efficient thermal interface has been integrated to the *f*-TEG, the output performances of *f*-TEG worn on human body could be substantially maximized. As shown in Fig. 7(b), the actual built ΔT across the whole *f*-TEG could reach 6 °C under static condition at room temperature of 23 °C, delivering a V_{OC} of 16.3 mV and further to 19.8 mV when a cotton wristlet was used to help preserve the body temperature. When wearing the *f*-TEG walking in real environment, the movement of the tester and the wind enhance heat dissipation with the air flow, resulting in dynamic yet much higher output varying between 25 and 37 mV.[14] The thermal interface design strategy, thus, essentially promotes the capability of *f*-TEG harvesting heat from body for practical power supply application.

Energy harvesting function from body heat has also been demonstrated via newly emerged TE materials-based *f*-TEGs, such as ductile semiconductors shown in Fig. 7(c). The super-thin TEG delivers a maximum normalized power density of ~30 $\mu W/cm^2 \cdot K^2$, benefiting from the high TE figure of merit of the materials and ultralow internal resistance of the device, e.g., ~18 m Ω for device with a filling factor of ~72%. Han *et al.* developed a gelatin-based ionic thermoelectric device that uses both thermal diffusion and redox reactions at two electrodes to generate a large thermopower. This device is capable of generating more than 2 V and a peak power of 5 μW from body heat.[89] These studies all show the promise of *f*-TEGs for sustainable power generation from low-grade thermal energy.

B. Temperature sensor

Another major application of *f*-TEG is the self-power temperature sensor, since it is capable of directly transmitting the electrical signal without any transduction, enabling easy integration of these temperature sensors in wearable electronics for real-time health monitoring.[20,142] Moreover, multifunctional sensor systems could be achieved when *f*-TEG is integrated with other sensing units with different functions.[21,143] We recently proposed a strategy to establish a vertically configured flexible pressure/temperature bimodal sensor array via a 3D architecture design on all-organic TE and piezoelectric materials employing laser structuring and printing techniques as shown in Fig. 8(a), presenting fast, highly sensitive, high selectivity, and wide sensing range tactile sensing ability as demonstrated in a practical human–machine interaction scenario as shown in Fig. 8(b). The ability to map the spatial distribution of both pressure and temperature response signals without interference of the sensor array is presented in Fig. 8(c).[22] The result is encouraging for developing *f*-TEGs toward broader application in multifunctional e-skin.

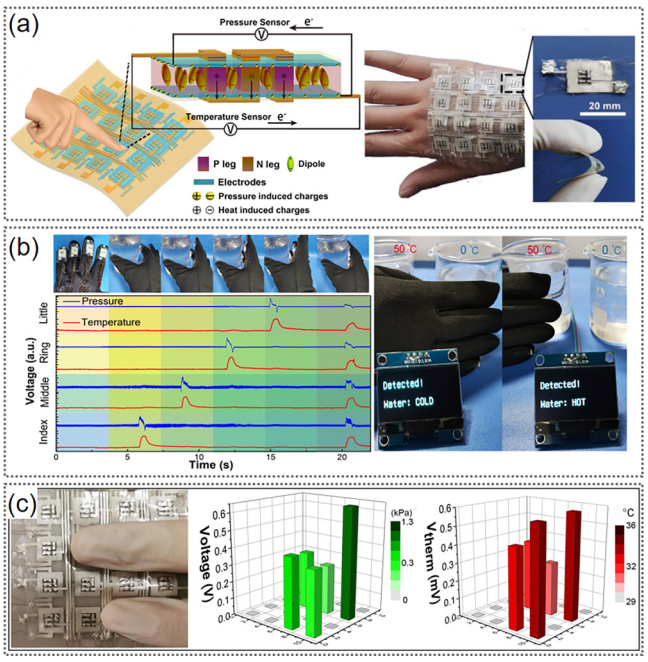

FIG. 8. (a) Demonstration on the piezo/thermoelectric bimodal tactile sensing principle of the e-skin. (b) An application scenario of the e-skin attached to a glove demonstrating real-time temperature/pressure signals in response to various finger motions of holding a warm cup. (c) Spatial mappings of bimodal sensing functions of the 4 × 4 pixel sensor array e-skin pressed by fingers in glove.[22]

C. Thermo-haptics

Virtual and augmented realities (VR/AR) reproduce a realistic and highly immersive experience by artificially reconstructing various human senses and delivering perceptual information to the sensory system; however, the critical challenge that hinder integration of VR/AR devices into everyday life and additional applications is related to the rigid and cumbersome form factor of current technology that is incompatible with dynamic movements and pliable limbs of the human body. Recent advancements in the fields of soft materials and wearable electronics are uniquely suited to provide solutions to this challenge. Thermal sensation, one of the tactile senses associated with the human skin, plays the most

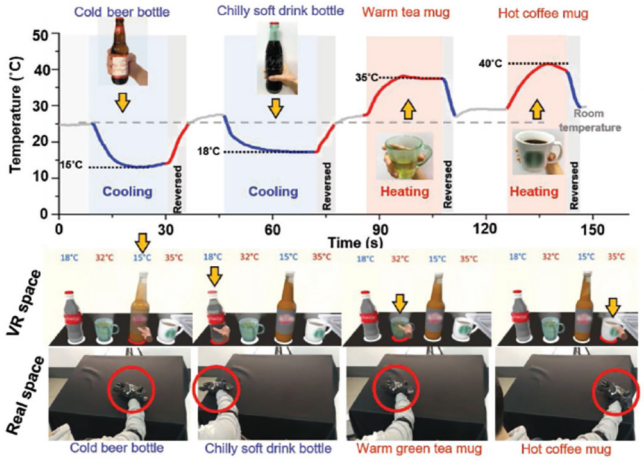

FIG. 9. Reconstruction of artificial thermal feeling with skin-like thermo-haptic device when touching various hot and cold objects in VR space. The top graph shows temperature change based upon the virtual scenario of touching various objects. The two sets of snapshots at the bottom correspond to the simultaneous motion of the hand in VR and real space, respectively, when touching objects at various temperature such as a chilly soda bottle, a mug of warm green tea, a mug of hot coffee, and a cold beer bottle (from left to right).[144]

significant role because of the constant heat exchange with other thermal entities via physical contact. In addition to simple temperature sensing, objects with different thermal conductivities, even at the same temperature, can be differentiated by the human body via touch. TEG could also be applied in the thermal management via a Peltier effect, in which changing the magnitude and direction of the electrical current allows the active control of the device temperature from cooling to heating, indicating its capability of controlling the desired temperature in a thermo-haptic system. Ko *et al.*[144] first developed a skin-like, highly soft and stretchable and bi-functional (both cold and hot sensation) thermo-haptic device for wearable VR applications with a single device structure, which was fabricated from thermally conductive elastomer encapsulated *p*- and *n*-type bismuth telluride thermoelectric pellets connected by serpentine Cu electrodes. They successfully demonstrated *in situ* data collection of temperature in a virtually realized scenario in which the user touched objects at different temperature such as a cold beer bottle, a chilly soda bottle, a mug of warm green tea, and a mug of hot coffee as shown in Fig. 9. It is expected that the development on flexible thermal VR/AR devices shall enhance the degree of artificial immersion and render VR/AR in a more authentic manner.[145]

V. SUMMARY AND OUTLOOK

Research efforts on thermoelectric materials composed of widely available elements, although less efficient, such as conducting polymers, carbon nanomaterials, or composites of these materials, have become a new subject of major interest in the scientific community in recent years driven by the need for low-grade heat harvesting and self-power supply for wearable electronics and IoTs sensors. Newly discovered thermoelectric materials and concepts capable of converting a heat flux into an electrical current by means of various types of particles transporting the electric charge, electrons, ions, and redox molecules, further enrich this rapid growing field.

Despite various prototypes of *f*-TEGs have been demonstrated to show promising power generation capability, very few of them could actually work without boost circuit or external power sources to drive electronics function, indicating that the actual output power from *f*-TEG is insufficient to fulfill the practical demand. It is essential to further enhance the power of *f*-TEG, including flexible materials with improved TE performance and their scalable integration into fully functional TEGs. Considering the trade-off between electrical properties, cost, massive production, and scalable integration, CNTs-based materials are of great potential. Recent report on the highly aligned carbon-nanotube shows ultrahigh power factors of 4091 and 4739 μW/m·K^2 for *p*- and *n*-type, respectively; and the integrated TEG successfully powers a red light-emitting diode using body heat alone, required no external power source.[146]

For practical application, stability and reliability of *f*-TEDs are of vital importance. For solution-processed flexible TE materials, their properties are largely determined by processing conditions and resultant polymorphic microstructures, which are not easy to precisely control, so there are great discrepancies on reported TE properties from group to group on a similar material system. The relationship between processing, microstructure, and properties of flexible TE materials is yet to be established. Massive studies on the evolution of mechanical, electrical, and thermal properties of all the materials included in the devices and their thermoelectric energy conversion function under working conditions from microscopic to macroscopic are required, as our understanding on the failure mechanism for various types of *f*-TEDs is quite limited currently.

Apart from the prosperous development of *f*-TEGs based on the Seebeck effect, Peltier devices for precise temperature control, which contributes a large market share in solid cooling industry, have been addressed to less extent in flexible devices, probably due to challenges in controlling the resistance of the *f*-TED at low level to overcome the Joule heat when current passes through and the significant effect of parasitic thermal resistance results from relative low thermal conductivity of either organic TE materials or elastomer encapsulation layer of the *f*-TED. Most importantly, the traditional heat sink structure is not applicable for *f*-TED, considering its wearability, alternative structures for efficient heat dissipation to maintain the cooling capability need further work with more efforts.

Extended reality (XR) technologies, including VR, AR, and MR (Mixed Reality), combine an enhanced physical reality with a virtual space to encompass them, are creating a brand new online ecology. Compared with advances of the XR software system, devices and materials' development remains in the very infancy stage, which is expected to artificially reconstruct various human feelings and transmit the information to human sensory systems. It may envision that adding the *f*-TED-based thermo-haptic device to other existing artificial sensings in XR devices broadens their application scope and improves the overall functionality, and demand from XR applications will further motivate technical advances for *f*-TEDs.

ACKNOWLEDGMENTS

This work was supported by the National Key Research and Development Program of China (Grant Nos. 2018YFA0702100 and 2018YFB0703600), the National Natural Science Foundation of China (Grant Nos. 92066203 and 51872009), and the Fundamental Research Funds for the Central Universities.

AUTHOR DECLARATIONS

Conflict of Interest

The authors have no conflicts to disclose.

Author Contributions

Yao Wang: Conceptualization (lead); Funding acquisition (equal); Supervision (lead); Writing – review & editing (lead). **Lu Yang:** Data curation (supporting); Writing – review & editing (supporting). **Yantao Zheng:** Data curation (supporting); Writing – review & editing (supporting). **Dangxiao Wang:** Conceptualization (supporting). **Yuan Deng:** Funding acquisition (equal); Project administration (supporting).

DATA AVAILABILITY

Data sharing is not applicable to this article as no new data were created or analyzed in this study.

REFERENCES

[1]L. E. Bell, Science **321**, 1457 (2008).
[2]J. He and T. M. Tritt, Science **357**, eaak9997 (2017).
[3]G. J. Snyder and E. S. Toberer, Nat. Mater. **7**, 105 (2008).
[4]F. J. DiSalvo, Science **285**, 703 (1999).
[5]P. Pichanusakorn and P. Bandaru, Mater. Sci. Eng.: R Rep. **67**, 19 (2010).
[6]M. Massetti, F. Jiao, A. J. Ferguson, D. Zhao, K. Wijeratne, A. Würger, J. L. Blackburn, X. Crispin, and S. Fabiano, Chem. Rev. **121**, 12465 (2021).
[7]L. Wang and K. Zhang, Energy Environ. Mater. **3**, 67 (2020).
[8]D. Zhang, Y. Wang, and Y. Yang, Small **15**, 1805241 (2019).
[9]R. Liu, Z. L. Wang, K. Fukuda, and T. Someya, Nat. Rev. Mater. **7**, 870 (2022).
[10]M. N. Hasan, M. Nafea, N. Nayan, and M. S. Mohamed Ali, Adv. Mater. Technol. **7**, 2101203 (2022).
[11]C. S. Kim, H. M. Yang, J. Lee, G. S. Lee, H. Choi, Y. J. Kim, S. H. Lim, S. H. Cho, and B. J. Cho, ACS Energy Lett. **3**, 501 (2018).
[12]Y. Wang, S. M. Zhang, and Y. Deng, J. Mater. Chem. A **4**, 3554 (2016).
[13]X. Shi, H. Chen, F. Hao, R. Liu, T. Wang, P. Qiu, U. Burkhardt, Y. Grin, and L. Chen, Nat. Mater. **17**, 421 (2018).
[14]Y. Wang, Z. Zhou, J. Zhou, L. Shao, Y. Wang, and Y. Deng, Adv. Energy Mater. **12**, 2102835 (2022).
[15]S. J. Kim, H. E. Lee, H. Choi, Y. Kim, J. H. We, J. S. Shin, K. J. Lee, and B. J. Cho, ACS Nano **10**, 10851 (2016).
[16]L. Francioso, C. De Pascali, R. Bartali, E. Morganti, L. Lorenzelli, P. Siciliano, and N. Laidani, ACS Appl. Mater. Interfaces **5**, 6586 (2013).
[17]Q. Yang, S. Yang, P. Qiu, L. Peng, T. Wei, Z. Zhang, X. Shi, and L. Chen, Science **377**, 854 (2022).
[18]Y. Yang, H. Hu, Z. Chen, Z. Wang, L. Jiang, G. Lu, X. Li, R. Chen, J. Jin, H. Kang, H. Chen, S. Lin, S. Xiao, H. Zhao, R. Xiong, J. Shi, Q. Zhou, S. Xu, and Y. Chen, Nano Lett. **20**, 4445 (2020).
[19]K. Nan, V. R. Feig, B. Ying, J. G. Howarth, Z. Kang, Y. Yang, and G. Traverso, Nat. Rev. Mater. **7**, 908 (2022).
[20]X. F. Zhao, S. Q. Yang, X. H. Wen, Q. W. Huang, P. F. Qiu, T. R. Wei, H. Zhang, J. C. Wang, D. W. Zhang, X. Shi, and H. L. Lu, Adv. Mater. **34**, 2107479 (2022).
[21]F. Zhang, Y. Zang, D. Huang, C. A. Di, and D. Zhu, Nat. Commun. **6**, 8356 (2015).
[22]P. Zhu, Y. Wang, Y. Wang, H. Mao, Q. Zhang, and Y. Deng, Adv. Energy Mater. **10**, 2001945 (2020).
[23]J. Xu, S. Wang, G. N. Wang, C. Zhu, S. Luo, L. Jin, X. Gu, S. Chen, V. Feig, J. W. F. To, S. Rondeau-Gagné, J. Park, B. C. Schroeder, C. Lu, J. Y. Oh, Y. Wang, Y. Kim, H. Yan, R. Sinclair, D. Zhou, G. Xue, B. Murmann, C. Linder, W. Cai, J. B. H. Tok, J. W. Chung, and Z. Bao, Science **355**, 59 (2017).
[24]S. Wang, J. Xu, W. Wang, G. N. Wang, R. Rastak, F. Molina-Lopez, J. W. Chung, S. Niu, V. R. Feig, J. Lopez, T. Lei, S. K. Kwon, Y. Kim, A. M. Foudeh, A. Ehrlich, A. Gasperini, Y. Yun, B. Murmann, J. B. H. Tok, and Z. Bao, Nature **555**, 83 (2018).
[25]Z. Fan, D. Du, X. Guan, and J. Ouyang, Nano Energy **51**, 481 (2018).
[26]Z. Fan, P. Li, D. Du, and J. Ouyang, Adv. Energy Mater. **7**, 1602116 (2017).
[27]K. Zhang, J. Qiu, and S. Wang, Nanoscale **8**, 8033 (2016).
[28]G. H. Kim, L. Shao, K. Zhang, and K. P. Pipe, Nat. Mater. **12**, 719 (2013).
[29]O. Bubnova, Z. U. Khan, A. Malti, S. Braun, M. Fahlman, M. Berggren, and X. Crispin, Nat. Mater. **10**, 429 (2011).
[30]N. Wen, Z. Fan, S. Yang, Y. Zhao, T. Cong, S. Xu, H. Zhang, J. Wang, H. Huang, C. Li, and L. Pan, Nano Energy **78**, 105361 (2020).
[31]N. Kim, S. Lienemann, I. Petsagkourakis, D. Alemu Mengistie, S. Kee, T. Ederth, V. Gueskine, P. Leclère, R. Lazzaroni, X. Crispin, and K. Tybrandt, Nat. Commun. **11**, 1424 (2020).
[32]S. Kee, M. A. Haque, D. Corzo, H. N. Alshareef, and D. Baran, Adv. Funct. Mater. **29**, 1905426 (2019).
[33]S. Qu, Q. Yao, L. Wang, Z. Chen, K. Xu, H. Zeng, W. Shi, T. Zhang, C. Uher, and L. Chen, NPG Asia Mater. **8**, e292 (2016).
[34]J. Li, X. Tang, H. Li, Y. Yan, and Q. Zhang, Synth. Met. **160**, 1153 (2010).
[35]Q. Yao, Q. Wang, L. Wang, Y. Wang, J. Sun, H. Zeng, Z. Jin, X. Huang, and L. Chen, J. Mater. Chem. A **2**, 2634 (2014).
[36]J. Wu, Y. Sun, W. B. Pei, L. Huang, W. Xu, and Q. Zhang, Synth. Met. **196**, 173 (2014).
[37]L. Liang, G. Chen, and C. Y. Guo, Mater. Chem. Front. **1**, 380 (2017).
[38]Y. J. Jeong, J. Jung, E. H. Suh, D. J. Yun, J. G. Oh, and J. Jang, Adv. Funct. Mater. **30**, 1905809 (2020).
[39]D. Huang, H. Yao, Y. Cui, Y. Zou, F. Zhang, C. Wang, H. Shen, W. Jin, J. Zhu, Y. Diao, W. Xu, C. A. Di, and D. Zhu, J. Am. Chem. Soc. **139**, 13013 (2017).
[40]Y. Sun, P. Sheng, C. Di, F. Jiao, W. Xu, D. Qiu, and D. Zhu, Adv. Mater. **24**, 932 (2012).
[41]D. Yuan, D. Huang, C. Zhang, Y. Zou, C. A. Di, X. Zhu, and D. Zhu, ACS Appl. Mater. Interfaces **9**, 28795 (2017).
[42]K. Wan, Z. Liu, B. C. Schroeder, G. Chen, G. Santagiuliana, D. G. Papageorgiou, H. Zhang, and E. Bilotti, Compos. Commun. **28**, 100952 (2021).
[43]B. Russ, M. J. Robb, F. G. Brunetti, P. L. Miller, E. E. Perry, S. N. Patel, V. Ho, W. B. Chang, J. J. Urban, M. L. Chabinyc, C. J. Hawker, and R. A. Segalman, Adv. Mater. **26**, 3473 (2014).
[44]L. Wang, Z. Zhang, Y. Liu, B. Wang, L. Fang, J. Qiu, K. Zhang, and S. Wang, Nat. Commun. **9**, 3817 (2018).
[45]H. Ju and J. Kim, ACS Nano **10**, 5730 (2016).
[46]Y. Lu, Y. Ding, Y. Qiu, K. Cai, Q. Yao, H. Song, L. Tong, J. He, and L. Chen, ACS Appl. Mater. Interfaces **11**, 12819 (2019).
[47]C. Liu, D. L. Shan, Z. H. Shen, G. K. Ren, Yue-Wang, Z. F. Zhou, J. Y. Li, D. Yi, J. L. Lan, L. Q. Chen, G. J. Snyder, Y. H. Lin, and C. W. Nan, Nano Energy **89**, 106380 (2021).
[48]W. S. Kim, G. Anoop, I. Jeong, H. J. Lee, H. B. Kim, S. H. Kim, G. W. Goo, H. Lee, H. J. Lee, C. Kim, J. Lee, B. S. Mun, J. W. Park, E. Lee, and J. Y. Jo, Nano Energy **67**, 104207 (2020).
[49]K. C. See, J. P. Feser, C. E. Chen, A. Majumdar, J. J. Urban, and R. A. Segalman, Nano Lett. **10**, 4664 (2010).

[50]Y. Liu, P. Liu, Q. Jiang, F. Jiang, J. Liu, G. Liu, C. Liu, Y. Du, and J. Xu, Chem. Eng. J. **405**, 126510 (2021).
[51]X. Wang, J. Cheng, L. Yin, Z. Zhang, X. Wang, J. Sui, X. Liu, J. Mao, F. Cao, and Q. Zhang, Adv. Funct. Mater. **32**, 2200307 (2022).
[52]J. A. Lee, A. E. Aliev, J. S. Bykova, M. J. de Andrade, D. Kim, H. J. Sim, X. Lepró, A. A. Zakhidov, J. B. Lee, G. M. Spinks, S. Roth, S. J. Kim, and R. H. Baughman, Adv. Mater. **28**, 5038 (2016).
[53]W. Hou, X. Nie, W. Zhao, H. Zhou, X. Mu, W. Zhu, and Q. Zhang, Nano Energy **50**, 766 (2018).
[54]Q. Jin, S. Jiang, Y. Zhao, D. Wang, J. Qiu, D. M. Tang, J. Tan, D. M. Sun, P. X. Hou, X. Q. Chen, K. Tai, N. Gao, C. Liu, H. M. Cheng, and X. Jiang, Nat. Mater. **18**, 62 (2019).
[55]Q. Jin, W. Shi, Y. Zhao, J. Qiao, J. Qiu, C. Sun, H. Lei, K. Tai, and X. Jiang, ACS Appl. Mater. Interfaces **10**, 1743 (2018).
[56]C. Wan, R. Tian, M. Kondou, R. Yang, P. Zong, and K. Koumoto, Nat. Commun. **8**, 1024 (2017).
[57]L. Wang, Z. Zhang, L. Geng, T. Yuan, Y. Liu, J. Guo, L. Fang, J. Qiu, and S. Wang, Energy Environ. Sci. **11**, 1307 (2018).
[58]C. Wan, X. Gu, F. Dang, T. Itoh, Y. Wang, H. Sasaki, M. Kondo, K. Koga, K. Yabuki, G. J. Snyder, R. Yang, and K. Koumoto, Nat. Mater. **14**, 622 (2015).
[59]J. Tang, R. Chen, L. Chen, G. C. Bazan, and Z. Liang, J. Mater. Chem. A **8**, 9797 (2020).
[60]Y. Chen, M. He, B. Liu, G. C. Bazan, J. Zhou, and Z. Liang, Adv. Mater. **29**, 1604752 (2017).
[61]Y. Wang, G. Liu, M. Sheng, C. Yu, and Y. Deng, J. Mater. Chem. A **7**, 1718 (2019).
[62]L. Yang, C. Liu, Y. Wang, P. Zhu, Y. Wang, and Y. Deng, Chin. Phys. B **31**, 028204 (2021).
[63]A. L. Pires, I. F. Cruz, J. Silva, G. N. P. Oliveira, S. Ferreira-Teixeira, A. M. L. Lopes, J. P. Araújo, J. Fonseca, C. Pereira, and A. M. Pereira, ACS Appl. Mater. Interfaces **11**, 8969 (2019).
[64]W. Zhao, S. Fan, N. Xiao, D. Liu, Y. Y. Tay, C. Yu, D. Sim, H. H. Hng, Q. Zhang, F. Boey, J. Ma, X. Zhao, H. Zhang, and Q. Yan, Energy Environ. Sci. **5**, 5364 (2012).
[65]J. Choi, Y. Jung, C. Dun, K. T. Park, M. P. Gordon, K. Haas, P. Yuan, H. Kim, C. R. Park, and J. J. Urban, ACS Appl. Energy Mater. **3**, 1199 (2020).
[66]T. Lee, K. T. Park, B. C. Ku, and H. Kim, Nanoscale **11**, 16919 (2019).
[67]B. A. MacLeod, N. J. Stanton, I. E. Gould, D. Wesenberg, R. Ihly, Z. R. Owczarczyk, K. E. Hurst, C. S. Fewox, C. N. Folmar, K. Holman Hughes, B. L. Zink, J. L. Blackburn, and A. J. Ferguson, Energy Environ. Sci. **10**, 2168 (2017).
[68]W. Zhou, Q. Fan, Q. Zhang, K. Li, L. Cai, X. Gu, F. Yang, N. Zhang, Z. Xiao, H. Chen, S. Xiao, Y. Wang, H. Liu, W. Zhou, and S. Xie, Small **12**, 3407 (2016).
[69]C. Zhang, Q. Zhang, D. Zhang, M. Wang, Y. Bo, X. Fan, F. Li, J. Liang, Y. Huang, R. Ma, and Y. Chen, Nano Lett. **21**, 1047 (2021).
[70]K. Suemori, Y. Watanabe, and S. Hoshino, Appl. Phys. Lett. **106**, 113902 (2015).
[71]D. Kim, Y. Kim, K. Choi, J. C. Grunlan, and C. Yu, ACS Nano **4**, 513 (2010).
[72]X. He, J. Shi, Y. Hao, M. He, J. Cai, X. Qin, L. Wang, and J. Yu, Carbon Energy **4**, 621 (2022).
[73]S. Mardi, K. Yusupov, P. M. Martinez, A. Zakhidov, A. Vomiero, and A. Reale, ACS Omega **6**, 1073 (2021).
[74]Q. Yao, Q. Wang, L. Wang, and L. Chen, Energy Environ. Sci. **7**, 3801 (2014).
[75]W. Ma, Y. Liu, S. Yan, T. Miao, S. Shi, Z. Xu, X. Zhang, and C. Gao, Nano Res. **11**, 741 (2018).
[76]D. Zhang, K. Zhang, Y. Wang, Y. Wang, and Y. Yang, Nano Energy **56**, 25 (2019).
[77]X. Sun, Y. Wang, K. Li, J. Wang, X. Dai, D. Chong, J. Yan, and H. Wang, Adv. Funct. Mater. **32**, 2203080 (2022).
[78]L. Tzounis, M. Petousis, S. Grammatikos, and N. Vidakis, Materials **13**, 2879 (2020).
[79]Y. Nonoguchi, K. Ohashi, R. Kanazawa, K. Ashiba, K. Hata, T. Nakagawa, C. Adachi, T. Tanase, and T. Kawai, Sci. Rep. **3**, 3344 (2013).
[80]Y. Nonoguchi, M. Nakano, T. Murayama, H. Hagino, S. Hama, K. Miyazaki, R. Matsubara, M. Nakamura, and T. Kawai, Adv. Funct. Mater. **26**, 3021 (2016).
[81]J. Choi, Y. Jung, S. J. Yang, J. Y. Oh, J. Oh, K. Jo, J. G. Son, S. E. Moon, C. R. Park, and H. Kim, ACS Nano **11**, 7608 (2017).
[82]Y. Wang, Z. Lu, Q. Hu, X. Qi, Q. Li, Z. Wu, H. Zhang, C. Yu, and H. Wang, J. Mater. Chem. A **9**, 3341 (2021).
[83]H. Wang, J. H. Hsu, S. I. Yi, S. L. Kim, K. Choi, G. Yang, and C. Yu, Adv. Mater. **27**, 6855 (2015).
[84]Y. T. Malik, Z. A. Akbar, J. Y. Seo, S. Cho, S. Y. Jang, and J. W. Jeon, Adv. Energy Mater. **12**, 2103070 (2022).
[85]Y. Fang, H. Cheng, H. He, S. Wang, J. Li, S. Yue, L. Zhang, Z. Du, and J. Ouyang, Adv. Funct. Mater. **30**, 2004699 (2020).
[86]Z. A. Akbar, J. W. Jeon, and S. Y. Jang, Energy Environ. Sci. **13**, 2915 (2020).
[87]H. Cheng, X. He, Z. Fan, and J. Ouyang, Adv. Energy Mater. **9**, 1901085 (2019).
[88]W. Gao, Z. Lei, C. Zhang, X. Liu, and Y. Chen, Adv. Funct. Mater. **31**, 2104071 (2021).
[89]C. G. Han, X. Qian, Q. Li, B. Deng, Y. Zhu, Z. Han, W. Zhang, W. Wang, S. P. Feng, G. Chen, and W. Liu, Science **368**, 1091 (2020).
[90]D. Zhao, H. Wang, Z. U. Khan, J. C. Chen, R. Gabrielsson, M. P. Jonsson, M. Berggren, and X. Crispin, Energy Environ. Sci. **9**, 1450 (2016).
[91]D. Zhao, A. Martinelli, A. Willfahrt, T. Fischer, D. Bernin, Z. U. Khan, M. Shahi, J. Brill, M. P. Jonsson, S. Fabiano, and X. Crispin, Nat. Commun. **10**, 1093 (2019).
[92]L. M. Goncalves, P. Alpuim, A. G. Rolo, and J. H. Correia, Thin Solid Films **519**, 4152 (2011).
[93]C. Yang, D. Souchay, M. Kneiß, M. Bogner, H. M. Wei, M. Lorenz, O. Oeckler, G. Benstetter, Y. Q. Fu, and M. Grundmann, Nat. Commun. **8**, 16076 (2017).
[94]L. X. Liang, Y. Deng, Y. Wang, H. L. Gao, and J. Cui, J. Nanopart. Res. **16**, 2575 (2014).
[95]S. Shin, R. Kumar, J. W. Roh, D. S. Ko, H. S. Kim, S. I. Kim, L. Yin, S. M. Schlossberg, S. Cui, J. M. You, S. Kwon, J. Zheng, J. Wang, and R. Chen, Sci. Rep. **7**, 7317 (2017).
[96]S. J. Kim, J. H. We, and B. J. Cho, Energy Environ. Sci. **7**, 1959 (2014).
[97]E. M. F. Vieira, J. Figueira, A. L. Pires, J. Grilo, M. F. Silva, A. M. Pereira, and L. M. Goncalves, J. Alloys Compd. **774**, 1102 (2019).
[98]Y. Ding, Y. Qiu, K. Cai, Q. Yao, S. Chen, L. Chen, and J. He, Nat. Commun. **10**, 841 (2019).
[99]Z. Gao, Q. Yang, P. Qiu, T. R. Wei, S. Yang, J. Xiao, L. Chen, and X. Shi, Adv. Energy Mater. **11**, 2100883 (2021).
[100]J. Liang, T. Wang, P. Qiu, S. Yang, C. Ming, H. Chen, Q. Song, K. Zhao, T. Wei, D. Ren, Y. Sun, X. Shi, J. He, and L. Chen, Energy Environ. Sci. **12**, 2983 (2019).
[101]S. Yang, Z. Gao, P. Qiu, J. Liang, T. R. Wei, T. Deng, J. Xiao, X. Shi, and L. Chen, Adv. Mater. **33**, 2007681 (2021).
[102]S. Xu, Z. Fan, S. Yang, X. Zuo, Y. Guo, H. Chen, and L. Pan, ACS Sens. **6**, 1120 (2021).
[103]H. J. Lee, G. Anoop, H. J. Lee, C. Kim, J. W. Park, J. Choi, H. Kim, Y. J. Kim, E. Lee, S. G. Lee, Y. M. Kim, J. H. Lee, and J. Y. Jo, Energy Environ. Sci. **9**, 2806 (2016).
[104]S. Mardi, M. Pea, A. Notargiacomo, N. Yaghoobi Nia, A. D. Carlo, and A. Reale, Materials **13**, 1404 (2020).
[105]R. Noriega, J. Rivnay, K. Vandewal, F. P. V. Koch, N. Stingelin, P. Smith, M. F. Toney, and A. Salleo, Nat. Mater. **12**, 1038 (2013).
[106]S. Mardi, P. Cataldi, A. Athanassiou, and A. Reale, Appl. Phys. Lett. **120**, 033102 (2022).
[107]S. Mardi, M. Risi Ambrogioni, and A. Reale, Mater. Res. Express **7**, 085101 (2020).
[108]N. E. Coates, S. K. Yee, B. McCulloch, K. C. See, A. Majumdar, R. A. Segalman, and J. J. Urban, Adv. Mater. **25**, 1629 (2013).
[109]Y. Wang, C. Yu, M. Sheng, S. Song, and Y. Deng, Adv. Mater. Interfaces **5**, 1701168 (2018).

[110]J. L. Blackburn, A. J. Ferguson, C. Cho, and J. C. Grunlan, Adv. Mater. **30**, 1704386 (2018).
[111]C. Bounioux, P. Díaz-Chao, M. Campoy-Quiles, M. S. Martín-González, A. R. Goñi, R. Yerushalmi-Rozen, and C. Müller, Energy Environ. Sci. **6**, 918 (2013).
[112]C. T. Hong, Y. H. Kang, J. Ryu, S. Y. Cho, and K. S. Jang, J. Mater. Chem. A **3**, 21428 (2015).
[113]L. Wang, J. Zhang, Y. Guo, X. Chen, X. Jin, Q. Yang, K. Zhang, S. Wang, and Y. Qiu, Carbon **148**, 290 (2019).
[114]S. Liu, H. Li, and C. He, Carbon **149**, 25 (2019).
[115]C. Cho, K. L. Wallace, P. Tzeng, J. Hsu, C. Yu, and J. C. Grunlan, Adv. Energy Mater. **6**, 1502168 (2016).
[116]B. Poudel, Q. Hao, Y. Ma, Y. Lan, A. Minnich, B. Yu, X. Yan, D. Wang, A. Muto, D. Vashaee, X. Chen, J. Liu, M. S. Dresselhaus, G. Chen, and Z. Ren, Science **320**, 634, (2008).
[117]T. R. Wei, M. Jin, Y. Wang, H. Chen, Z. Gao, K. Zhao, P. Qiu, Z. Shan, J. Jiang, R. Li, L. Chen, J. He, and X. Shi, Science **369**, 542 (2020).
[118]S. H. Park, S. Jo, B. Kwon, F. Kim, H. W. Ban, J. E. Lee, D. H. Gu, S. H. Lee, Y. Hwang, J. S. Kim, D. B. Hyun, S. Lee, K. J. Choi, W. Jo, and J. S. Son, Nat. Commun. **7**, 13403 (2016).
[119]S. Jo, S. Choo, F. Kim, S. H. Heo, and J. S. Son, Adv. Mater. **31**, 1804930 (2019).
[120]Y. He, X. Lin, Y. Feng, B. Luo, and M. Liu, Adv. Sci. **9**, 2204675 (2022).
[121]S. Hwang, W. J. Potscavage, R. Nakamichi, and C. Adachi, Org. Electron. **31**, 31 (2016).
[122]C. A. Hewitt, A. B. Kaiser, S. Roth, M. Craps, R. Czerw, and D. L. Carroll, Nano Lett. **12**, 1307 (2012).
[123]T. Sun, J. L. Peavey, M. David Shelby, S. Ferguson, and B. T. O'Connor, Energy Convers. Manag. **103**, 674 (2015).
[124]B. Russ, A. Glaudell, J. J. Urban, M. L. Chabinyc, and R. A. Segalman, Nat. Rev. Mater. **1**, 16050 (2016).
[125]F. Suarez, D. P. Parekh, C. Ladd, D. Vashaee, M. D. Dickey, and M. C. Öztürk, Appl. Energy **202**, 736 (2017).
[126]P. Zhu, C. Shi, Y. Wang, Y. Wang, Y. Yu, Y. Wang, Y. Deng, and J. Xiao, Adv. Energy Mater. **11**, 2100920 (2021).
[127]Y. Du, K. Cai, S. Chen, H. Wang, S. Z. Shen, R. Donelson, and T. Lin, Sci. Rep. **5**, 6411 (2015).
[128]T. Sun, B. Zhou, Q. Zheng, L. Wang, W. Jiang, and G. J. Snyder, Nat. Commun. **11**, 572 (2020).
[129]Y. Zheng, X. Han, J. Yang, Y. Jing, X. Chen, Q. Li, T. Zhang, G. Li, H. Zhu, H. Zhao, G. J. Snyder, and K. Zhang, Energy Environ. Sci. **15**, 2374 (2022).
[130]J. Choi, E. W. Zaia, M. Gordon, and J. J. Urban, Curr. Trends Fashion Technol. Textile Eng. **2**, 555583 (2018).
[131]A. Zhang, G. Li, B. Wang, and J. Wang, J. Electron. Mater. **50**, 1514 (2021).
[132]Q. Zhou, K. Zhu, J. Li, Q. Li, B. Deng, P. Zhang, Q. Wang, C. Guo, W. Wang, and W. Liu, Adv. Sci. **8**, 2004947 (2021).
[133]F. Suarez, A. Nozariasbmarz, D. Vashaee, and M. C. Öztürk, Energy Environ. Sci. **9**, 2099 (2016).
[134]V. Padmanabhan Ramesh, Y. Sargolzaeiaval, T. Neumann, V. Misra, D. Vashaee, M. D. Dickey, and M. C. Ozturk, Npj Flex. Electron. **5**, 1 (2021).
[135]K. Zhu, B. Deng, P. Zhang, H. S. Kim, P. Jiang, and W. Liu, Energy Environ. Sci. **13**, 3514 (2020).
[136]N. H. Trung, N. Van Toan, and T. Ono, J. Micromech. Microeng. **27**, 125006 (2017).
[137]B. Lee, H. Cho, K. T. Park, J. S. Kim, M. Park, H. Kim, Y. Hong, and S. Chung, Nat. Commun. **11**, 5948 (2020).
[138]Y. Sargolzaeiaval, V. Padmanabhan Ramesh, T. V. Neumann, V. Misra, D. Vashaee, M. D. Dickey, and M. C. Öztürk, Appl. Energy **262**, 114370 (2020).
[139]M. G. Cooper, B. B. Mikic, and M. M. Yovanovich, Int. J. Heat Mass Transfer **12**, 279 (1969).
[140]M. Bahrami, J. R. Culham, M. M. Yovanovich, and G. E. Schneider, Heat Transf. Summer Conf. **36959**, 411 (2003).
[141]H. N. Ho and L. A. Jones, in *14th Symposium on Haptic Interfaces for Virtual Environment and Teleoperator Systems* (IEEE, 2006), p. 461.
[142]J. C. Yang, J. Mun, S. Y. Kwon, S. Park, Z. Bao, and S. Park, Adv. Mater. **31**, 1904765 (2019).
[143]Y. Wang, H. Mao, Y. Wang, P. Zhu, C. Liu, and Y. Deng, J. Mater. Chem. A **8**, 15167 (2020).
[144]J. Lee, H. Sul, W. Lee, K. R. Pyun, I. Ha, D. Kim, H. Park, H. Eom, Y. Yoon, J. Jung, D. Lee, and S. H. Ko, Adv. Funct. Mater. **30**, 1909171 (2020).
[145]J. Lee, D. Kim, H. Sul, and S. H. Ko, Adv. Funct. Mater. **31**, 2007376 (2021).
[146]K. T. Park, Y. S. Cho, I. Jeong, D. Jang, H. Cho, Y. Choi, T. Lee, Y. Ko, J. Choi, S. Y. Hong, M.-W. Oh, S. Chung, C. R. Park, and H. Kim, Adv. Energy Mater. **12**, 2200256 (2022).